

On the co-orbital motion of two planets in quasi-circular orbits

Philippe Robutel and Alexandre Pousse

IMCCE, Observatoire de Paris, UPMC, CNRS UMR8028, 77 Av. Denfert-Rochereau, 75014 Paris, France

May 26, 2022

ABSTRACT

We develop an analytical Hamiltonian formalism adapted to the study of the motion of two planets in co-orbital resonance. The Hamiltonian, averaged over one of the planetary mean longitude, is expanded in power series of eccentricities and inclinations. The model, which is valid in the entire co-orbital region, possesses an integrable approximation modeling the planar and quasi-circular motions. First, focusing on the fixed points of this approximation, we highlight relations linking the eigenvectors of the associated linearized differential system and the existence of certain remarkable orbits like the elliptic Eulerian Lagrangian configurations, the Anti-Lagrange (Giuppone et al., 2010) orbits and some second sort orbits discovered by Poincaré. Then, the variational equation is studied in the vicinity of any quasi-circular periodic solution. The fundamental frequencies of the trajectory are deduced and possible occurrence of low order resonances are discussed. Finally, with the help of the construction of a Birkhoff normal form, we prove that the elliptic Lagrangian equilateral configurations and the Anti-Lagrange orbits bifurcate from the same fixed point L_4 .

Subject headings: Co-orbitals; Resonance; Lagrange; Euler; Planetary problem; Three-body problem

1. Introduction

The co-orbital resonance has been extensively studied for more than one hundred years in the framework of the restricted three-body problem (RTBP). In most of the analytical works, the emphasis has been placed on the tadpole orbits, trajectories surrounding one of the two Lagrangian triangular equilibrium points, since these describe the motion of the Jovian Trojans. However, the global topology of the co-orbital resonance has been studied in particular by Garfinkel (1976, 1978) and Érdi (1977), but the interest for the horseshoe orbits which encompass the three equilibrium points L_3 , L_4 and L_5 , remained academic until the discovery of the Saturnian satellites Janus and Epimetheus (Smith et al. 1980; Synnott et al. 1981). In Dermott and Murray (1981a), general properties of the tadpole and horseshoe orbits are described in the quasi-circular case. In particular, asymptotic estimates of the horseshoe orbits lifetime and the relative width of this orbits domain are given. But the impossibility to get explicit expressions of the horseshoe orbits complicated their study, and theoretical works were replaced by numerical simulations. Thereby, Christou (2000) showed that the region containing the tadpole orbits is not disconnected from the horseshoe one, and that there exist transitions between these two domains. Also, a global study of the phase space of the co-orbital resonance was presented in the RTPB by Nesvorný et al. (2002) using a numerical averaging of the disturbing function over orbital frequencies. Using the same kind of numerical technics, Giuppone et al. (2010) studied the stability regions and families of periodic orbits of two planets locked in the co-orbital resonance. Besides the Lagrangian triangular configurations, where the three bodies in Keplerian motion

occupy the vertices of an equilateral triangle, these authors found a new family of fixed points (equilibrium in the reduced average problem, but quasi-periodic with two fundamental frequencies for the non-average problem in inertial reference frame) that they called Anti-Lagrange orbits. Both Lagrange and Anti-Lagrange families can be seen as a one-parameter family of stable fixed points, parametrized by the eccentricity. As shown in the Fig. 7 of Giuppone et al. (2010), when the eccentricity is equal to zero, the corresponding configurations of each family seem to merge in the well known circular Lagrangian equilateral configuration. Finally, when the eccentricity increases, the stability regions surrounding these orbits become smaller, the one associated to the Lagrangian configuration being the first to vanish.

In this paper, we will develop a Hamiltonian formalism adapted to the study of the motion of two planets in co-orbital resonance. We modify the methods presented in Laskar and Robutel (1995) in order to get an analytical expansion of the planetary Hamiltonian averaged over an orbital period, meaning averaged over one of the planetary mean longitudes. This expansion, which is a power series of the eccentricities and inclinations whose coefficients depend on the semi-major axes and on the difference of the planetary mean longitudes, generalizes the expressions obtained in the RTBP framework by Morais (1999, 2001). Moreover, this one containing only even terms in the eccentricities and inclinations (see Section 2), the planar circular motions are conserved along the solutions. These quasi-circular co-orbital motions are modeled by an integrable Hamiltonian depending only on the semi-major axes and the mean longitudes difference. Contrary to the integrable approximations derived by Yoder et al. (1983) or Morais (1999, 2001), our model possesses five fixed points. Three are unstable and correspond to the Eulerian collinear configurations denoted by L_1 , L_2 and L_3 where the two planets revolve on circles centered at the Sun. The two others correspond to the circular Lagrangian equilateral configurations L_4 and L_5 mentioned above, which are linearly stable if the planetary masses are small enough (Gascheau 1843).

In Section 3, the linear differential system associated to infinitesimal variations transversal to the plane containing the quasi-circular orbits will be studied. Only the directions corresponding to the eccentricities will be considered. First, focusing on the fixed points, we will highlight relations linking the eigenvectors of the linearized differential system and the existence of certain remarkable orbits like the elliptic Eulerian and the Lagrangian configurations, the Anti-Lagrange orbits and some second sort orbits discovered by Poincaré (1892). Then, the variational equation will be studied in the vicinity of any quasi-circular periodic solution. The fundamental frequencies of the trajectory will be deduced, and possible occurrence of low order resonances will be discussed.

Section 4 will be devoted to the construction of a Birkhoff normal form in the neighborhood of L_4 . Beside the derivation of the fundamental frequencies of any quasi-periodic trajectory lying in this neighborhood, we will prove that the elliptic Lagrangian equilateral configurations and the Anti-Lagrange orbits bifurcate from the same fixed point L_4 . Finally, in Section 5, comments and various approaches for future works will be presented.

2. The average Hamiltonian

2.1. Canonical heliocentric coordinates

We consider two planets of respective masses m_1 and m_2 orbiting a central body (Sun, or star) of mass m_0 dominant with respect to the planetary masses. As only co-orbital planets are considered, no planet is permanently farther from the central body than the other, so the heliocentric coordinate system seems to be the most adapted to this situation. Following Laskar and Robutel (1995), the Hamiltonian of the three-body

problem reads

$$\begin{aligned}
 H(\tilde{\mathbf{r}}_j, \mathbf{r}_j) &= H_K(\tilde{\mathbf{r}}_j, \mathbf{r}_j) + H_p(\tilde{\mathbf{r}}_j, \mathbf{r}_j) \quad \text{with} \\
 H_K(\tilde{\mathbf{r}}_j, \mathbf{r}_j) &= \sum_{j \in \{1,2\}} \left(\frac{\tilde{\mathbf{r}}_j^2}{2\beta_j} - \frac{\mu_j \beta_j}{\|\mathbf{r}_j\|} \right) \quad \text{and} \\
 H_p(\tilde{\mathbf{r}}_j, \mathbf{r}_j) &= \frac{\tilde{\mathbf{r}}_1 \cdot \tilde{\mathbf{r}}_2}{m_0} - \mathcal{G} \frac{m_1 m_2}{\|\mathbf{r}_1 - \mathbf{r}_2\|},
 \end{aligned} \tag{1}$$

where \mathbf{r}_j is the heliocentric position of the planet j , $\beta_j = m_0 m_j (m_0 + m_j)^{-1}$ and $\mu_j = \mathcal{G} (m_0 + m_j)$, \mathcal{G} being the gravitational constant. The conjugated variable of \mathbf{r}_j , denoted by $\tilde{\mathbf{r}}_j$, is the barycentric linear momentum of the body of index j . In this expression, H_K corresponds to the unperturbed Keplerian motion of the two planets, more precisely the motion of a mass β_j around a fixed center of mass $m_0 + m_j$, while H_p models the gravitational perturbations. If we introduce the small parameter ε given by

$$\varepsilon = \text{Max} \left(\frac{m_1}{m_0}, \frac{m_2}{m_0} \right), \tag{2}$$

one can verify that the Keplerian term of the planetary Hamiltonian is of order ε and the other one is of order ε^2 which justifies a perturbative approach.

The choice of these canonical heliocentric coordinates $(\tilde{\mathbf{r}}_j, \mathbf{r}_j)$ may lead to quite surprising results for quasi-circular motions. In particular, the famous Lagrangian relative equilibrium, where the three bodies occupying the vertices of an equilateral triangle animated with an uniform rotation, is described in terms of elliptical elements by ellipses in rapid rotation. More precisely, $\tilde{\mathbf{r}}_j$ being not collinear to the heliocentric velocity of the planet j , the Keplerian motion associated to the unperturbed Hamiltonian $\tilde{\mathbf{r}}_j^2/(2\beta_j) - \mu_j \beta_j / \|\mathbf{r}_j\|$ is not represented by a circle described with constant angular velocity, but by a rapidly precessing ellipse whose eccentricity is proportional to the planetary masses. This phenomenon described in the appendix (Section 6) is similar to the question of the definition of elliptical elements for a satellite orbiting an oblate body (see Greenberg (1981)). Except this little drawback which occurs only when the considered motion is close to the circular Lagrangian configurations, the canonical heliocentric variables are particularly well suited to the study of the co-orbital resonances.

In order to define a canonical coordinate system related to the elliptical elements $(a_j, e_j, I_j, \lambda_j, \varpi_j, \Omega_j)$ (respectively the semi-major axis, the eccentricity, the inclination, the mean longitude, the longitude of the pericenter and the longitude of the ascending node of the planet j), we start from Poincaré's rectangular variables in complex form $(\lambda_j, \Lambda_j, x_j, -i\bar{x}_j, y_j, -i\bar{y}_j)$ where $\Lambda_j = \beta_j \sqrt{\mu_j a_j}$,

$$\begin{aligned}
 x_j &= \sqrt{\Lambda_j} \sqrt{1 - \sqrt{1 - e_j^2}} \exp(i\varpi_j), \\
 y_j &= \sqrt{\Lambda_j} \sqrt{\sqrt{1 - e_j^2} (1 - \cos I_j)} \exp(i\Omega_j).
 \end{aligned} \tag{3}$$

This coordinate system has the advantage of being regular when the eccentricities and the inclinations tend to zero. It is also convenient to use the non-dimensional quantities $X_j = x_j \sqrt{2/\Lambda_j}$ and $Y_j = y_j / \sqrt{2\Lambda_j}$ which are equivalent to $e_j \exp(i\varpi_j)$ and $I_j \exp(i\Omega_j)/2$ for quasi-planar and quasi-circular motions.

As we only consider the planetary motions in the vicinity of the circular planar problem, the Hamiltonian can be expanded in power series of the variables X_j, Y_j and their conjugates in the form

$$\sum_{k_1, k_2} \left(\sum_{(\mathbf{p}, \mathbf{q}) \in \mathbb{N}^8} \Psi_{\mathbf{p}, \mathbf{q}}^{k_1, k_2} (\Lambda_1, \Lambda_2) X_1^{p_1} X_2^{p_2} \bar{X}_1^{\bar{p}_1} \bar{X}_2^{\bar{p}_2} Y_1^{q_1} Y_2^{q_2} \bar{Y}_1^{\bar{q}_1} \bar{Y}_2^{\bar{q}_2} \right) e^{i(k_1 \lambda_1 + k_2 \lambda_2)}, \tag{4}$$

where the integers occurring in these summations satisfy the relation

$$\sum_j (k_j + p_j + q_j - \bar{p}_j - \bar{q}_j) = 0, \quad (5)$$

known as D'Alembert rule. This relation corresponds to the invariance of the Hamiltonian by rotation, or, which is equivalent, to the fact that the angular momentum of the system is an integral of the motion. Remark that we will not use this explicit Fourier expansion in this paper, but the D'Alembert rule will play an important role.

According to Poincaré (1905), the expression of the angular momentum in Poincaré's variables reads

$$\mathbf{C} = \sum_j \mathbf{r}_j \times \tilde{\mathbf{r}}_j = \sum_j \begin{pmatrix} \sqrt{2}\Im(y_j)\sqrt{\Lambda_j - |x_j|^2 - \frac{|y_j|^2}{2}} \\ -\sqrt{2}\Re(y_j)\sqrt{\Lambda_j - |x_j|^2 - \frac{|y_j|^2}{2}} \\ \Lambda_j - |x_j|^2 - |y_j|^2 \end{pmatrix}. \quad (6)$$

In order to deal with the co-orbital resonance, an appropriate canonical coordinate system is¹ $(\theta_j, J_j, x_j, -i\bar{x}_j, y_j, -i\bar{y}_j)$ with

$$\begin{aligned} \theta_1 &= \lambda_1 - \lambda_2, & 2J_1 &= \Lambda_1 - \Lambda_2, \\ \theta_2 &= \lambda_1 + \lambda_2, & 2J_2 &= \Lambda_1 + \Lambda_2. \end{aligned} \quad (7)$$

Inside the 1:1 mean motion resonance, the angular variable θ_1 varies slowly with respect to θ_2 . Consequently, the planetary Hamiltonian (1) will be averaged over the angle θ_2 .

2.2. The quasi-circular and planar average problem

2.2.1. The average problem

In this paper, we only consider the average Hamiltonian at first order in the planetary masses. More precisely, we assume that there exists a canonical transformation which maps the initial Hamiltonian H to

$$\bar{H}(\theta_j, J_j, x_j, -i\bar{x}_j, y_j, -i\bar{y}_j) = \bar{H}_0(J_j) + \bar{H}_1(\theta_1, J_j, x_j, -i\bar{x}_j, y_j, -i\bar{y}_j) + \mathcal{O}(\varepsilon^3) \quad (8)$$

with

$$\bar{H}_0(J_1, J_2) = -\frac{\beta_1^3 \mu_1^2}{2(J_1 + J_2)^2} - \frac{\beta_2^3 \mu_2^2}{2(J_1 - J_2)^2} = H_K \circ \phi(\theta_j, J_j, x_j, -i\bar{x}_j, y_j, -i\bar{y}_j) \quad (9)$$

and

$$\bar{H}_1(\theta_1, J_j, x_j, -i\bar{x}_j, y_j, -i\bar{y}_j) = \frac{1}{2\pi} \int_0^{2\pi} H_p \circ \phi(\theta_j, J_j, x_j, -i\bar{x}_j, y_j, -i\bar{y}_j) d\theta_2, \quad (10)$$

where the map ϕ satisfy the relation $(\tilde{\mathbf{r}}_j, \mathbf{r}_j) = \phi(\theta_j, J_j, x_j, -i\bar{x}_j, y_j, -i\bar{y}_j)$. If we denote by $(\theta_j, J_j, x_j, -i\bar{x}_j, y_j, -i\bar{y}_j)$ the canonical variables associated to the average problem, we remark that $J_2 = \Lambda_1 + \Lambda_2$ is a first integral of \bar{H} . It is also easy to prove that the quantities $\sum_j y_j \sqrt{\Lambda_j - |x_j|^2 - |y_j|^2/2}$ and $\sum_j [\Lambda_j - |x_j|^2 - |y_j|^2]$ are first integrals too. It is possible to take advantage of these first integrals by reducing the problem by

¹Other coordinates adapted to the co-orbital resonance have been used by several authors (e.g. Nesvorný et al. (2002) for the RTBP and Giuppone et al. (2010) for the planetary problem), but these systems, that performed the reduction of the angular momentum, are singular when the eccentricities tend to zero.

means of adapted canonical coordinate system as it is the case with the Jacobi reduction in the spatial problem (see Robutel (1995) and Malige et al. (2002)). The reduction can also be achieved in the planar problem leading to two degrees of freedom Hamiltonian system depending on two angles: the difference of the mean longitudes and the difference of the longitudes of the perihelion (Giuppone et al. (2010)). These reductions introducing some technical issues (addition of a parameter, singularities when the eccentricities and inclinations tend to zero), we prefer not to reduce the problem.

The average Hamiltonian (10) depending on the mean longitude only by their difference θ_1 , the rotational invariance of the Hamiltonian given by the relation (5) imposes that \overline{H} is even in the variables x_j and y_j and their conjugates. As a consequence, the set $x_1 = x_2 = y_1 = y_2 = 0$ is an invariant manifold by the flow of the average Hamiltonian (10). More generally, this property holds for any order of averaging. This implies that the part of the average Hamiltonian (10) which does not depend on the eccentricities and the inclinations, namely $H_0(\theta_1, J_j) = \overline{H}(\theta_1, J_j, 0, 0, 0, 0)$, is an integrable Hamiltonian. It is worth noting that the one degree of freedom Hamiltonian H_0 , associated to the circular and planar resonant problem, is a peculiar attribute of the 1:1 mean-motion resonance. The next section is devoted to its study.

2.2.2. The integrable part H_0

After replacing the vectors \mathbf{r}_j and $\tilde{\mathbf{r}}_j$ by their expressions in terms of elliptic elements into the planetary Hamiltonian (1), an explicit expression of H_0 is obtained by suppressing the terms depending on the variables $x_j, \bar{x}_j, y_j, \bar{y}_j$ and the fast angle θ_2 . This leads to the Hamiltonian

$$H_0 = -\frac{\beta_1 \mu_1}{2a_1} - \frac{\beta_2 \mu_2}{2a_2} + \mathcal{G} m_1 m_2 \left(\frac{\cos \theta_1}{\sqrt{a_1 a_2}} - \frac{1}{\sqrt{a_1^2 + a_2^2 - 2a_1 a_2 \cos \theta_1}} \right), \quad (11)$$

where the semi-major axis a_j depends on the action J_1 and the first integral J_2 . The constant $2J_2 = \Lambda_1 + \Lambda_2$ being positive, there exists a strictly positive number \bar{a} such that

$$J_2 = \frac{\beta_1 \sqrt{\mu_1} + \beta_2 \sqrt{\mu_2}}{2} \sqrt{\bar{a}}. \quad (12)$$

At this point, it is convenient to define a new couple of conjugate variables (θ, J) by translating the action J_1 as

$$J_1 = \frac{\beta_1 \sqrt{\mu_1} - \beta_2 \sqrt{\mu_2}}{2} \sqrt{\bar{a}} + J, \quad \theta_1 = \theta. \quad (13)$$

It will also be useful to define the dimensionless (non canonical) action-like variable u by the relation

$$J = (\beta_1 + \beta_2) \sqrt{\mu_0 \bar{a}} u \quad \text{with} \quad \mu_0 = \mathcal{G} m_0. \quad (14)$$

Now, by a substitution of the relations

$$a_j = \left(\sqrt{\bar{a}} + \frac{(-1)^{j+1}}{\beta_j \sqrt{\mu_j}} J \right)^2 = \bar{a} \left(1 + (-1)^{j+1} \frac{\beta_1 + \beta_2}{\beta_j} \sqrt{\frac{\mu_0}{\mu_j}} u \right)^2 \quad (15)$$

into the expression (11), the integrable average Hamiltonian H_0 can be explicitly expressed in terms of the (θ, J, \bar{a}) , or (θ, u, \bar{a}) for convenience. Note that the expression (15) allows one to interpret the parameter \bar{a} as a mean value around which the semi-major axes oscillate.

The figure 1 reproduces the phase portrait of the integrable Hamiltonian H_0 in coordinates (θ, u) . It can easily be expressed in terms of semi-major axes using the expression (15) or their first order approximation $a_j - \bar{a} \approx [2(-1)^{j+1}\bar{a}(m_1 + m_2)/m_j] u$. The upper plot represents the whole phase diagram for $m_1 = m_J = 10^{-3}$ and $m_2 = m_S = 3 \times 10^{-4}$ and $\mathcal{G} = m_0 = \bar{a} = 1$, where the masses m_J and m_S are close to those of Jupiter and Saturn expressed in solar mass. This plot is similar to the well known Hill's diagram (or zero-velocity curves) of the non averaged planar circular RTBP (see Szebehely (1967)) although the zero-velocity curves are not solution curves of the motion. It is also topologically equivalent to the phase space of the average planar circular RTBP when the eccentricity of the test-particle is equal to zero (Nesvorný et al. 2002; Morbidelli 2002). The Hamiltonian system associated to H_0 possesses five fixed points that correspond to the usual Euler and Lagrangian configurations, and one singular point at $u = \theta = 0$ which corresponds to the collision between the planets. The two stable equilibrium points located at $\theta = \pm\pi/3, u = 0$ (see the next paragraph for more details) represent the average equilateral configurations that we will denote abusively by L_4 and L_5 by analogy with the RTBP. Each of these points is surrounded by tadpole orbits corresponding to periodic deformations of the equilateral triangle. This region is bounded by the separatrix \mathcal{S}_3 that originates at the hyperbolic fixed point L_3 at $\theta = \pi, u \approx 0$, for which the three bodies are aligned and the Sun is between the two planets and its separatrix. Outside of this domain, the horseshoe orbits are enclosed by the separatrix \mathcal{S}_2 that originates at the fixed point L_2 ($\theta = 0$ and $u < 0$). This point, as the equilibrium point L_1 , is associated with an Euler configuration for which the two planets are on the same side of the Sun. The last domain, centered at the singularity, is surrounded by the separatrix \mathcal{S}_1 connecting the L_1 point ($\theta = 0$ and $u > 0$) to itself. Inside this small region, the two planets seem to be subjected to a prograde satellite-like motion, the one revolving the other one clockwise. By an enlargement of this region ($-0.1 < \theta < 0.1$), the second plot of Fig. 1 (middle box) shows the splitting of the two separatrices \mathcal{S}_1 (red) and \mathcal{S}_2 (blue) when the planetary masses are different. On the contrary, for equal planetary masses, the phase portrait becomes symmetric with respect to the axis $u = 0$. It turns out that the equilibrium points L_3, L_4, L_5 lie on the axis of symmetry, and that the two curves \mathcal{S}_1 and \mathcal{S}_2 merge together giving rise to a unique separatrix connecting L_1 to L_2 . The bottom plot of Fig. 1 describes this phenomenon for $m_1 = m_2 = 5 \times 10^{-4}$, the other parameters being unchanged.

A way to estimate the locations of the equilibrium points is to use an asymptotic expansion of the Hamiltonian (11) in the neighborhood of $u = 0$. Two cases have to be considered. The first one arises in a domain which excludes a suitable neighborhood of the collision (the distance between the planets has to be of order unity). The second case concerns a small domain enclosing the singularity. In the first situation, our goal can be achieved by an expansion of the Hamiltonian (11) in the neighborhood $u = 0$, assuming that the condition $\theta = \mathcal{O}(1)$ is fulfilled. We will see later that this is satisfied in the tadpole region. This condition also holds for the horseshoe orbits which do not approach too much the singularity. Denoting by Γ the quantity $\sqrt{2 - 2\cos\theta}$, and using the notations $\sigma_1 = m_1 + m_2$, $\sigma'_1 = m_1 - m_2$ and $\sigma_2 = m_1 m_2$, the expansion of H_0 can be written as

$$H_0(\theta, u) = \mathcal{G}\bar{a}^{-1} [\gamma_1 + \gamma_2(\theta) + \mathcal{O}(\varepsilon^3) + (\delta_2(\theta) + \mathcal{O}(\varepsilon^3)) u + (\tau_1 + \tau_2(\theta) + \mathcal{O}(\varepsilon^3)) u^2 + u^3 R(\theta, u, \varepsilon)] , \quad (16)$$

where the coefficients $\gamma_k, \tau_k, \delta_k$ are given by

$$\begin{aligned} 2\gamma_1 &= -m_0\sigma_1, & 2\gamma_2 &= \sigma_2(2 - \Gamma^2 - 2\Gamma^{-1}), \\ 2\delta_2 &= -\sigma_1\sigma'_1(1 - \Gamma)^2(1 + 2\Gamma^{-1}), & 2\tau_1 &= -3m_0\sigma_1^3\sigma_2^{-1}, \\ \tau_2 &= \sigma_1^2\sigma_2^{-1} [(\sigma_1^2 - 3\sigma_2)(4 - \Gamma^2/2 - \Gamma^{-1}) + 2\sigma_1^2\Gamma^{-3}] , \end{aligned} \quad (17)$$

and the remainder R is a periodic function of θ depending on u and of order ε . The location of the

fixed points L_3 , L_4 and L_5 , as well as the eigenvalues of the associated linearized system, can be easily deduced from the expansion (16). The location of the two elliptic fixed points L_4 and L_5 is approximated by $(\theta, u) = (\pm\pi/3, 0 + \mathcal{O}(\varepsilon^2))$, which leads to $a_1 = \bar{a}(1 + \mathcal{O}(\varepsilon^2))$, $a_2 = \bar{a}(1 + \mathcal{O}(\varepsilon^2))$. The quadratic expansion of the Hamiltonian H_0 in the neighborhood of L_4 (change $\pi/3$ in $-\pi/3$ for L_5) is equal to

$$H_{0,L_4}^{(2)} = -\frac{3}{2} \frac{\mathcal{G}}{\bar{a}} \left(\frac{\sigma_1^2}{\sigma_2} (m_0 \sigma_1 - 3\sigma_1^2 + 5\sigma_2) u^2 + \frac{3}{4} \sigma_2 \left(\theta - \frac{\pi}{3} \right)^2 \right), \quad (18)$$

where only the dominating terms in ε are retained. Moreover, the frequency associated to this elliptic fixed point reads

$$\nu_0 = n_0 \sqrt{\frac{27}{4} \frac{\sigma_1}{m_0}} \left(1 - \frac{\sigma_1^2 - \sigma_2}{2m_0 \sigma_1} + \mathcal{O}(\varepsilon^2) \right), \quad (19)$$

where $n_0 = \mu_0^{1/2} \bar{a}^{-3/2}$ plays the role of an averaged mean motion. The location of the hyperbolic point L_3 is obtained by translating u by a quantity $u^{(3)}$ which cancels the linear term in u in the expansion (16) when $\theta = \pi$. We get the approximation

$$u^{(3)} = -\frac{(m_1 - m_2)m_1 m_2}{3m_0(m_1 + m_2)^2} + \mathcal{O}(\varepsilon^2), \quad (20)$$

which gives in terms of semi-major axes:

$$a_j = \bar{a} \left(1 + \frac{(-1)^j}{3} \frac{m_k}{m_0} \frac{m_1 - m_2}{m_1 + m_2} + \mathcal{O}(\varepsilon^2) \right) \quad \text{with} \quad j \neq k. \quad (21)$$

As a consequence, the quadratic expansion of H_0 in the vicinity of L_3 , whose coordinates are $(\pi, u^{(3)})$, reads

$$H_{0,L_3}^{(2)} = -\frac{3}{2} \frac{\mathcal{G}}{\bar{a}} \left(\frac{\sigma_1^2}{\sigma_2} (m_0 \sigma_1 - \frac{7}{6} \sigma_1^2 + 3\sigma_2) (u - u^{(3)})^2 - \frac{7}{24} \sigma_2 (\theta - \pi)^2 \right). \quad (22)$$

The domain including the tadpole orbits is bounded by the separatrix \mathcal{S}_3 . The size of this domain can be estimated by different ways. A simple manner to achieve this goal is to calculate the quantity U_3 which is the maximal value taken by the action u along \mathcal{S}_3 . By solving the equation $H_0(\pi/3, U_3) = H_0(\pi, u^{(3)})$ where H_0 is approximated by (16), we get the expression:

$$U_3 = \frac{\sqrt{2}\sigma_2}{\sqrt{3m_0\sigma_1^3}} + \mathcal{O}(\varepsilon^2) = \frac{\sqrt{2}m_1 m_2}{\sqrt{3m_0(m_1 + m_2)^3}} + \mathcal{O}(\varepsilon^2). \quad (23)$$

Similarly, in the perpendicular direction, we can also estimate the quantity Θ_3 corresponding to the minimal value of θ along \mathcal{S}_3 by an approximation of the positive root of the equation $H_0(\Theta_3, 0) = H_0(\pi, u^{(3)})$. The solution is given by

$$\Theta_3 = 2 \arcsin\left(\frac{\sqrt{2}-1}{2}\right) + \mathcal{O}(\varepsilon) \approx 23.9^\circ, \quad (24)$$

which is a classical result in the case of the RTBP (Garfinkel 1977).

The approximation (16) is not valid for the Euler points L_1 and L_2 , the latter being located at a distance of order $\varepsilon^{1/3}$ of the singularity. In this case, we can use the asymptotic expansion of $H_0(0, u)$, valid since $u = \mathcal{O}(\varepsilon^\alpha)$ with $0 \leq \alpha < 1$, given by

$$H_0(0, u) = \mathcal{G}\bar{a}^{-1} \left[\gamma'_{-1} |u|^{-1} + \gamma'_1 + \gamma'_2 + \mathcal{O}(\varepsilon^3) + (\delta'_2 + \mathcal{O}(\varepsilon^3)) u + (\tau'_1 + \tau'_2 + \mathcal{O}(\varepsilon^3)) u^2 + u^3 R'(u, \varepsilon) \right], \quad (25)$$

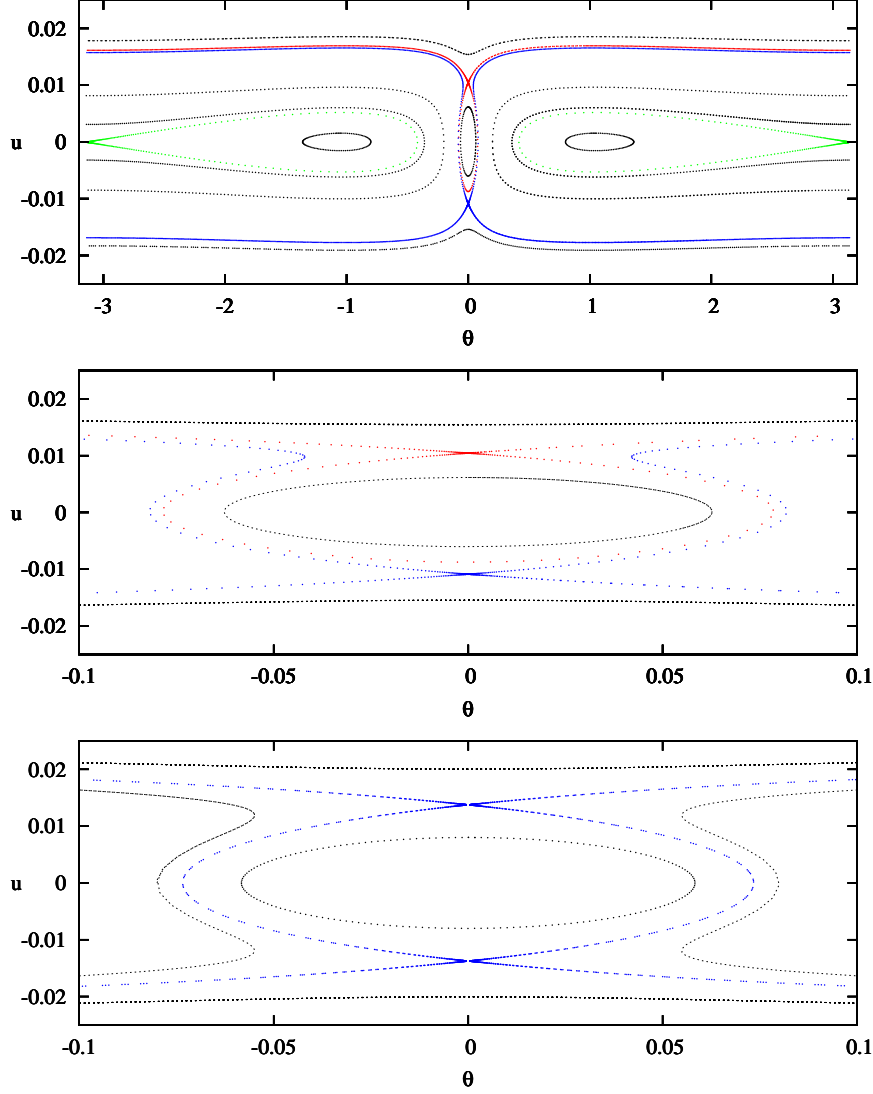


Fig. 1.— Phase portrait of the Hamiltonian H_0 in coordinates (θ, u) . The upper box shows the whole space for $m_0 = 1$, $m_1 = m_J$ and $m_2 = m_S$, the parameters \mathcal{G} and \bar{a} being equal to one. The separatrix that originates at L_3 (\mathcal{S}_3) is plotted in green, while \mathcal{S}_2 is the blue curve and \mathcal{S}_1 the red one. The middle plot is an enlargement of the region surrounding the collision point while the bottom plot shows the merging of the two separatrices \mathcal{S}_1 and \mathcal{S}_2 when the planetary masses are equal. Here, their values are $m_1 = m_2 = 5 \times 10^{-4}$.

where the coefficients $\gamma_k, \tau_k, \delta_k$ are

$$\begin{aligned}
 2\gamma'_{-1} &= -\sigma_1^{-2}\sigma_2^2, & 2\gamma'_1 &= 2\gamma_1 = -m_0\sigma_1, & \gamma'_2 &= \sigma_2, \\
 2\delta_2 &= 3\sigma_1\sigma'_1, & 2\tau_1 &= 2\tau'_1 = -3m_0\sigma_1^3\sigma_2^{-1}, \\
 \tau'_2 &= 4(\sigma_1^2 - 3\sigma_2)\sigma_1^2\sigma_2^{-1}
 \end{aligned} \tag{26}$$

and R' is a periodic function of θ depending on u and of order ε . At this accuracy, the two Euler points L_1 and L_2 are symmetric with respect to the line $u = 0$, and if we denote by $u^{(1)}$ (resp. $u^{(2)}$) the u -coordinate of L_1 (resp. L_2), we have $u^{(2)} = -u^{(1)} + \mathcal{O}(\varepsilon^{2/3})$ and

$$u^{(1)} = \frac{\sigma_2}{(6m_0\sigma_1^5)^{1/3}} + \mathcal{O}(\varepsilon^{2/3}) = \frac{m_1m_2}{(6m_0(m_1+m_2)^5)^{1/3}} + \mathcal{O}(\varepsilon^{2/3}). \quad (27)$$

Let us mention that the quantities $u^{(1)}$, $u^{(2)}$ and $u^{(3)}$ can also be considered as roots of a polynomial equation, as it is the case for Euler's configurations in the full three-body problem (see Marchal and Bozis (1982) or Roy (1982)).

As for the tadpole orbits, the width of the horseshoe region along the u axis can be deduced from the equation $H_0(\pi/3, U_1) = H_0(0, u^{(1)})$ that is

$$U_1 = 2^{-1/2}6^{1/6}m_0^{-1/3}\sigma_1^{-5/3}\sigma_2 + \mathcal{O}(\varepsilon^{2/3}). \quad (28)$$

The minimal angular separation between two planets in horseshoe orbit is solution of the equation $H_0(\theta^{(1)}, 0) = H_0(0, u^{(1)})$, and is equivalent to

$$\theta^{(1)} = \frac{4}{3} \left(\frac{\sigma_1}{6m_0} \right)^{1/3} + \mathcal{O}(\varepsilon^{2/3}). \quad (29)$$

We note that at this degree of accuracy (neglecting the terms of order $\varepsilon^{2/3}$), the two separatrices \mathcal{S}_1 and \mathcal{S}_2 merged in a single curve.

The equations (23) and (28) allow one to retrieve the result on the relative size of the tadpole and horseshoe regions obtained by Dermott and Murray (1981a) in a very different way. Indeed, we have

$$\frac{U_3}{U_1} = 2\sqrt[6]{6} \left(\frac{m_1+m_2}{m_0} \right)^{1/6} = \mathcal{O}(\varepsilon^{1/6}). \quad (30)$$

As a consequence, the lower the planetary masses are, the larger the horseshoe region is (with respect to the width of the tadpole region).

It is worth to mention that, although the average system modeled by the Hamiltonian H_0 provides a faithful representation of the topology of the problem, it only reflects poorly the dynamics in the domain bounded by \mathcal{S}_1 containing the singularity.

The simplest argument that points out this problem comes from the computation of the orbit frequency surrounding the collision point. Indeed, close to the singularity, the Hamiltonian can be approximated by

$$-\mathcal{G}m_1m_2\bar{a}^{-1}(\alpha J^2 + \theta^2)^{-1/2} \quad \text{with} \quad \alpha = (m_1m_2\mu_0\bar{a})^{-1}. \quad (31)$$

It turns out that the frequency of the trajectory that originates at $\theta = \theta_0$ and $J = 0$ is equivalent to

$$\frac{\sqrt{m_1m_2}}{m_0} \frac{n_0}{\theta_0^3}. \quad (32)$$

As a product of an averaging process, this frequency would be small compared to n_0 , but it tends to infinity when θ_0 tends to zero.

To conclude this section, we will compare the average Hamiltonian H_0 to a classical approximation of the co-orbital resonance. This model, represented by the Hamiltonian H_a which reads

$$H_a = -\frac{3}{2} \frac{\mathcal{G}}{\bar{a}} \frac{m_0(m_1+m_2)^3}{m_1m_2} u^2 + \frac{\mathcal{G}m_1m_2}{\bar{a}} \left(\cos\theta - \frac{1}{\sqrt{2-2\cos\theta}} \right), \quad (33)$$

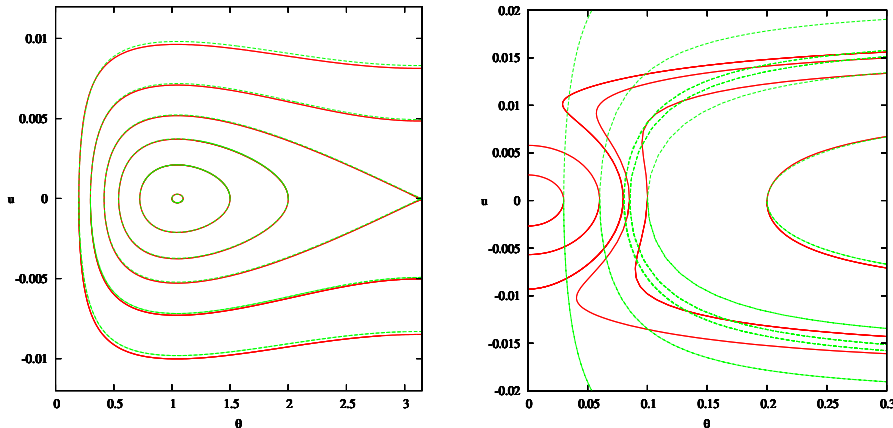


Fig. 2.— Comparison between the model H_0 and its approximation H_a . The level curves of H_0 are plotted in red while the level curves of H_a are in green. The two approximations fit correctly when the trajectories do not come too close to the singularity (left panel). The right plot shows the inconsistency between the two models in the Hill region.

has been used by Yoder et al. (1983) to study the dynamics of the co-orbital satellites Janus and Epimetheus (see also Sicardy and Dubois (2003)). A similar Hamiltonian is also employed to model the 1:1 mean motion resonance in the RTBP (see Morais (1999)). This approximation is a particular case of the expression (16) obtained by expanding H_0 in power series of u and ε . For small enough values of u , and if θ is not too close to 0 or to 2π , the Hamiltonian H_a provides a good approximation of H_0 in the tadpole region and for horseshoe orbits providing $u \ll \varepsilon^{1/3}$. As one can see on the left plot of the figure 2, although the differential system associated to the Hamiltonian H_a possesses only three fixed points, its trajectories are very close to those of the average Hamiltonian H_0 , when they do not approach the collision. This is especially true for the tadpole orbits and the moderate amplitude horseshoe orbits. On the contrary, as shown in Fig. 2 (right panel), the second model is not valid in the Hill region. But we have to keep in mind that though in this region the topology of the average problem is well described by H_0 , it is not the case of its dynamics.

3. Variational equations in the neighborhood of the quasi-circular problem

3.1. The variational equations

It has been shown in the previous section that the manifold $x_j = y_j = 0$ is invariant by the flow of the average Hamiltonian (10). In order to study the (linear) stability of this invariant manifold in the transversal directions (x_j, y_j) , we have to calculate the variational equations associated to this invariant surface. These equations, corresponding to the linearization of the differential system associated to the Hamiltonian (10) in the neighborhood of the plane $x_j = y_j = 0$, can be derived from the quadratic expansion in eccentricity and inclination of the average Hamiltonian \bar{H} . This expansion can be written in the form $H_0 + H_2^{(h)} + H_2^{(v)}$ with

$$H_2^{(h)} = \mathcal{G}m_1m_2 (A_h X_1 \bar{X}_1 + B_h X_1 \bar{X}_2 + \bar{B}_h \bar{X}_1 X_2 + A_h X_2 \bar{X}_2) \quad (34)$$

and

$$H_2^{(v)} = \mathcal{G}m_1m_2 (A_v Y_1 \bar{Y}_1 + B_v Y_1 \bar{Y}_2 + \bar{B}_v \bar{Y}_1 Y_2 + A_v Y_2 \bar{Y}_2), \quad (35)$$

where the coefficients A_h, B_h, A_v and B_v read

$$\begin{aligned}
 A_v &= \left(\frac{a_1 a_2}{\Delta^3} - \frac{1}{\sqrt{a_1 a_2}} \right) \cos \theta, & B_v &= \left(\frac{1}{\sqrt{a_1 a_2}} - \frac{a_1 a_2}{\Delta^3} \right) e^{i\theta}, \\
 A_h &= \frac{a_1 a_2}{8\Delta^5} (a_1 a_2 (5 \cos 2\theta - 13) + 4(a_1^2 + a_2^2) \cos \theta) - \frac{\cos \theta}{2\sqrt{a_1 a_2}}, \\
 B_h &= \frac{e^{-2i\theta}}{2\sqrt{a_1 a_2}} - \frac{a_1 a_2}{16\Delta^5} (a_1 a_2 (e^{-3i\theta} + 9e^{i\theta} - 26e^{-i\theta}) + 8(a_1^2 + a_2^2)e^{-2i\theta}), \\
 \Delta &= \sqrt{a_1^2 + a_2^2 - 2a_1 a_2 \cos \theta}.
 \end{aligned} \tag{36}$$

The formulas (34), (35) and (36) generalize the expansion given by Morais (1999, 2001) in the case of the elliptic RTBP.

The variational equations in the vicinity of a solution lying in the plane $x_j = y_j = 0$ and satisfying

$$\dot{\theta} = \frac{1}{c} \frac{\partial H_0}{\partial u}(\theta, u), \quad \dot{u} = -\frac{1}{c} \frac{\partial H_0}{\partial \theta}(\theta, u) \quad \text{with} \quad c = (\beta_1 + \beta_2) \sqrt{\mu_0 \bar{a}}, \tag{37}$$

take the form

$$\begin{pmatrix} \dot{X}_1 \\ \dot{X}_2 \end{pmatrix} = 2i\mathcal{G}m_1 m_2 \begin{pmatrix} \Lambda_1^{-1} A_h & \Lambda_1^{-1} \bar{B}_h \\ \Lambda_2^{-1} B_h & \Lambda_2^{-1} A_h \end{pmatrix} \begin{pmatrix} X_1 \\ X_2 \end{pmatrix} = M_h(\theta, u) \begin{pmatrix} X_1 \\ X_2 \end{pmatrix} \tag{38}$$

and

$$\begin{pmatrix} \dot{Y}_1 \\ \dot{Y}_2 \end{pmatrix} = \frac{i\mathcal{G}m_1 m_2}{2} \begin{pmatrix} \Lambda_1^{-1} A_v & \Lambda_1^{-1} \bar{B}_v \\ \Lambda_2^{-1} B_v & \Lambda_2^{-1} A_v \end{pmatrix} \begin{pmatrix} Y_1 \\ Y_2 \end{pmatrix} = M_v(\theta, u) \begin{pmatrix} Y_1 \\ Y_2 \end{pmatrix}, \tag{39}$$

where θ and u are deduced from the solutions of the equations (37), and the Λ_j implicitly depend on u by the relations (15). As these solutions are periodic (except if their initial conditions are chosen on the separatrices \mathcal{S}_1 to \mathcal{S}_3) the linear equations (38) and (39) are periodically time-dependent. As a consequence, their solutions cannot generally be expressed in a close form. A notable exception occurs at the equilibrium points of the system (37). Indeed, here, the variational equations become autonomous and consequently integrable. Then we will first begin to study these special cases. Before going further, let us mention that in this paper, we will not study the ‘‘vertical’’ variational equation (39). Indeed, due to its strong degeneracy, the study of this linear equation is not sufficient to understand the local dynamics. To this aim, the use of higher order terms of the Hamiltonian is necessary (at least the fourth degree in y_j). To be convinced, it is enough to look at the matrix M_v , defined in (39), for $\theta = \pi/3$ and $u = 0$. Indeed, at L_4 the matrix vanishes and the quadratic Hamiltonian does not provide any information about the dynamics in the y_j directions. Then, this situation requires a careful analysis of the structure of the Hamiltonian in order to deal with potential bifurcations in the vertical direction, as it is pointed out by Jorba (2000) in the case of the bicircular problem. Therefore, we postpone this study to a future work.

3.1.1. Dynamics around the fixed points

For the equilateral configurations ($\theta = \pm\pi/3$), neglecting the quadratic terms in ε , the matrix M_h takes the following expression

$$M_h = -i \frac{27}{8} \frac{n_0}{m_0} \begin{pmatrix} m_2 & -m_2 e^{i\theta} \\ -m_1 e^{-i\theta} & m_1 \end{pmatrix}. \tag{40}$$

This matrix possesses two eigendirections associated to the eigenvectors

$$V_1 = \begin{pmatrix} e^{i\theta} m_2 \\ -m_1 \end{pmatrix} \quad \text{and} \quad V_2 = \begin{pmatrix} e^{i\theta} \\ 1 \end{pmatrix}, \quad (41)$$

whose eigenvalues are respectively

$$v_1 = -i \frac{27}{8} \frac{m_1 + m_2}{m_0} n_0 \quad \text{and} \quad v_2 = 0. \quad (42)$$

These eigenvectors have a precise physical meaning. Along the neutral direction, the one which is collinear with V_2 , the two eccentricities are the same and the angle $\Delta\varpi = \varpi_1 - \varpi_2$ separating the two apsidal lines is equal to $\pi/3$ at L_4 and $-\pi/3$ at L_5 . These configurations clearly correspond to the Lagrangian elliptic equilibria, which are fixed points of the average problem, and consequently of the linearized average problem at L_4 or L_5 . This is the reason why the associated eigenvalue v_2 vanishes. Along the direction V_1 , the orbits satisfy the relations

$$a_1 = a_2 = \bar{a}, \quad \theta = \pm\pi/3, \quad m_1 e_1 = m_2 e_2, \quad \text{and} \quad \Delta\varpi = \varpi_1 - \varpi_2 = \theta + \pi. \quad (43)$$

This corresponds to an infinitesimal version of the Anti-Lagrange orbits found numerically by Giuppone et al. (2010). On these trajectories the elliptic elements a_1, a_2, e_1, e_2 and θ are constant. Only the two angles ϖ_1 and ϖ_2 precess with the same frequency equal to

$$g_1 = i v_1 = \frac{27}{8} \frac{m_1 + m_2}{m_0} n_0, \quad (44)$$

in such a way that the angle $\Delta\varpi$ is constant. As a consequence, this family of periodic orbits is transformed, after reduction by the rotations, in a family of fixed points, which is exactly what have found Giuppone et al. (2010) in the reduced problem. Of course, the family that we found along the eigenvector V_1 of the linearized system provides only an infinitesimal approximation of the Anti-Lagrange family in the neighborhood of L_4 , but we will show in Section 4 that this linear approximation can be generalized to any degree using Birkhoff normal form.

3.1.2. The Eulerian fixed point L_3

By evaluating the matrix $M_h(\theta, u)$ at $(\theta, u) = (\pi, u^{(3)})$ and neglecting the terms in ε^2 and more, the matrix of the linearized system at L_3 reads

$$M'_h = i \frac{7}{8} \frac{n_0}{m_0} \begin{pmatrix} m_2 & m_2 \\ m_1 & m_1 \end{pmatrix}. \quad (45)$$

This matrix possesses two eigendirections associated to the eigenvectors

$$V'_1 = \begin{pmatrix} m_2 \\ m_1 \end{pmatrix} \quad \text{and} \quad V'_2 = \begin{pmatrix} 1 \\ -1 \end{pmatrix}, \quad (46)$$

whose eigenvalues are respectively

$$v'_1 = i \frac{7}{8} \frac{m_1 + m_2}{m_0} n_0 \quad \text{and} \quad v'_2 = 0. \quad (47)$$

As in the equilateral case, the direction V_2' corresponds to the unstable Euler configurations where the two planets are in the two sides of the Sun (the eccentricities are equal and the perihelia are in opposition). The other direction is more interesting. In this case, the perihelia are in conjunction and the eccentricities verify the relation $m_1 e_1 = m_2 e_2$. As for L_4 , the method developed in Section 4.1 makes possible to prove the existence of a one-parameter family of periodic orbits that bifurcates from L_3 and is tangent to V_1' at this point. Remark that, at least close to L_3 , this family has been numerically computed by Hadjidemetriou et al. (2009), and were previously found by Poincaré (1892) as a solution of second sort ² (see Chenciner (2012)).

3.1.3. Euler L_1 and L_2 equilibria

As the Hamiltonian H_0 does not reflect properly the dynamics in the neighborhood of the collision between the two planets, the linearized problem at L_1 or L_2 will not be considered in the present paper (see the end of Section 2.2.2).

3.2. The general solution of the variational equation

Now, let us study the general case. This corresponds to writing the variational equation (38) around a periodic solution of frequency ν . According to the Floquet theorem (see Meyer and Hall (1992)), the solutions of the variational equation take the form

$$z(t) = P(\nu t) \exp(At), \quad (48)$$

where A is a constant matrix and $P(\psi)$ is a matrix whose coefficients are 2π -periodic functions of ψ . As, if Z is a fundamental matrix solution to the variational equation along a $2\pi/\nu$ -periodic solution, one has the relation

$$Z(t + 2\pi\nu^{-1}) = Z(t) \exp(2\pi\nu^{-1}A), \quad (49)$$

and the solutions stability of the variational equation depends on the eigenvalues of the monodromy matrix $\exp(2\pi\nu^{-1}A)$. As a consequence, if we start the integration at $t = 0$ from the identity matrix, after a period, we get the relation $\exp(2\pi\nu^{-1}A) = Z(2\pi\nu^{-1})$. Thus, this matrix and its eigenvalues can be deduced from a simple numerical integration of the variational equation. If the eigenvalues modulus of this matrix are equal to one, the solutions of (38) are quasi-periodic. Moreover, their fundamental frequencies are ν, g_1, g_2 , where g_1 and g_2 are equal to the eigenvalues arguments of the monodromy matrix multiplied by $\nu/(2\pi)$. Fig. 3 shows the results corresponding to planetary masses $m_1 = m_J$ and $m_2 = m_S$. From the numerical computations of the monodromy matrix eigenvalues, we conclude that solutions of the variational equation are always quasi-periodic, and thus the invariant manifold of the quasi-circular orbits $x_1 = x_2 = 0$ is transversally stable, at least in the directions associated to the eccentricities. This property seems to hold for every value of planetary masses that we have tested, that is $m_1 = m_2 = 10^{-p}$ and $m_2 = 0.3 \times m_1 = 0.3 \times 10^{-p}$ with p ranging for 3 to 8. Figure 3 shows the behavior of the frequencies ν, g_1 and g_2 along a section of the space phase. The red curve corresponds to ν , the green one to g_1 and the blue one to g_2 . The initial conditions are chosen on the segment $\theta = \pi/3$ and $0 \leq u \leq u^{(1)}$, $u^{(1)}$ being defined by the relation (27) as the positive intersection of the line $\theta = \pi/3$ with the separatrix \mathcal{S}_1 . This plot shows clearly two different dynamical

²Méthodes nouvelles de la mécanique celeste Vol I, Chap III, &47: "Solutions de la seconde sorte".

domains: the inner one filled with tadpole orbits ranging from $u = 0$ to $u^{(3)}$, and the outer domain for $u^{(3)} < u < u^{(1)}$ populated by horseshoe orbits.

Inside the inner region, the libration frequency ν decreases from the value $\nu^0 \approx \sqrt{27(m_1 + m_2)/(4m_0)}n_0 \approx 0.0936 \text{ yr}^{-1}$ to zero when the separatrix \mathcal{S}_3 is reached. The frequency g_1 associated to the precession of the periastra evolves smoothly between $27(m_1 + m_2)n_0/(8m_0) \approx 0.00439 \text{ yr}^{-1}$ at L_4 and $7(m_1 + m_2)n_0/(8m_0) \approx 0.00114 \text{ yr}^{-1}$ approaching \mathcal{S}_3 . The box located in the upper left corner of the plot details its evolution for $0 < u < 0.0055$. As shown in this figure, the last frequency g_2 is always very small with respect to the other ones. It starts from zero and reaches zero again at the separatrix, being at least always twenty times smaller than g_1 . Because in the tadpole region, the frequency ν is of order $\sqrt{\varepsilon}$ and g_1 of order ε , these two frequencies do not generate low order resonances (some of these resonances are indicated by vertical black dotted lines), except in a very narrow neighborhood of \mathcal{S}_3 . As ν tends to zero at \mathcal{S}_3 , in both sides of this separatrix, the two curves intersect and ν becomes smaller than g_1 . Using the estimates derived by Garfinkel (1976, 1978) in the RTBP, one can easily show that the frequency ν reaches a logarithmic singularity where it tends to zero as $-(\log|u - u^{(3)}|)^{-1}$. Consequently, the slope of the curve associated to ν is very steep and then the low order resonances occur only very close to the separatrix, in a region which is intrinsically unstable.

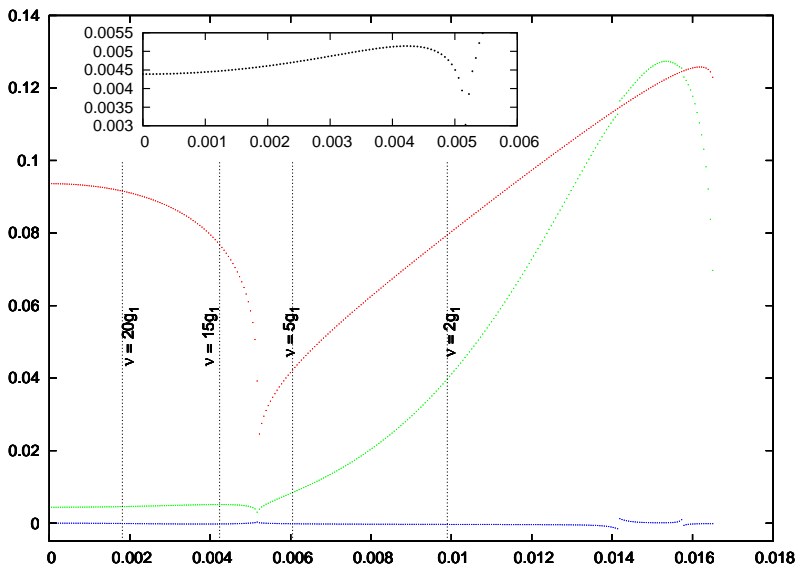


Fig. 3.— Variations of the fundamental frequencies of the variational equation. u is plotted along the X-axis and the frequencies, in rad/yr, along the Y-axis. The red curve represents the evolution of the libration frequency ν along the segment $\theta = \pi/3$, $0 \leq u < u^{(1)}$, while the green (resp. blue) curve is associated to g_1 (resp. g_2). The vertical black dotted lines indicate the location on some resonances between g_1 and ν . The box plotted in the upper left corner of the figure is an enlargement showing the behavior of g_1 for $0 \leq u < 0.0055$.

The situation is more interesting inside the horseshoe domain. Indeed, if g_2 remains always very small

with respect to the frequency g_1 , this one increases significantly after the crossing of the separatrix \mathcal{S}_3 . Note that this behavior is already mentioned by Morais (1999) where the figure 1.a of her paper dedicated to the RTBP corresponds approximately to our figure 3 for u ranging from 0 to about 0.008. After this value, g_1 keeps to increase, reaching the resonance $\nu = 2g_1$ at $u \approx 0.01$ and even the 1:1 resonance between ν and g_1 approaching the end of the horseshoe domain materialized by the separatrix \mathcal{S}_1 . After the crossing of the two curves representing the frequencies ν and g_1 , g_1 remains temporarily above ν . The situation is reversed quickly as ν tends to zero when \mathcal{S}_1 is reached.

The behavior of the three fundamental frequencies ν, g_1, g_2 , described for $m_1 = m_J$ and $m_2 = m_S$, seems to be very weakly mass-dependent. Indeed, the simulations performed with the mass sample presented above converge to the same conclusions. First, the frequency g_2 is always small with respect to g_1 and of course to ν . Second, no significant resonance which may destabilize the average system occurs in the tadpole region, excepted in a narrow area surrounding \mathcal{S}_3 : the lower the planetary masses are, the larger the ratio ν/g_1 is. And third, in the horseshoe domain, low order resonances involving ν and g_1 always occur, in particular, the 1:1 close to \mathcal{S}_1 is crossed two times. If these low order resonances generate chaotic behaviors in the average problem, it is not necessarily this mechanism that dominates in the full (non averaged) three-body problem for planetary masses comparable to those of Jupiter or Saturn. Indeed, Laughlin and Chambers (2002) deduced from numerical simulations of the planetary three-body problem that horseshoe orbits, even starting with the two planets in circular motion, are unstable for planetary masses satisfying the empirical relation $(m_1 + m_2)/(m_0 + m_1 + m_2) > 0.0004$. This limit corresponding approximately to two Saturn’s mass planets around the Sun. One can find comparable simulations in different cases in Dvorak (2006). In a nice paper by Barrarés and Ollé (2006), this behavior is studied more carefully. In the case of the RTBP, these authors prove that the invariant manifolds associated to L_3 deeply penetrate the region populated by horseshoe orbits, generating a large chaotic region, whose size increases with the mass of the secondary (the mass of the primary being fixed). They even mentioned the possible heteroclinic intersections with the invariant manifolds associated to Lyapunov orbits around L_1 and L_2 . A similar mechanism probably acts in the planar planetary problem. As suggested by C. Simó (private communication), not only L_3 invariant manifolds, but also invariant objects of periodic orbits existing in the vicinity of the previous manifolds are supposed to be involved in the process, as it is the case in the spatial RTBP. This phenomenon, acting in short time-scale, plays a major role in the instability of the horseshoe regions, even for zero initial eccentricities. For moderate to small planetary masses, the portion of the horseshoe orbit region intersecting the invariant manifolds mentioned above shrinks to a narrow region, excluding transitions between the L_3 region and the neighborhoods of L_1 and L_2 . In absence of short time-scale chaos, the destabilizing effect of the resonances involving the frequencies ν and g_j can dominate, at least locally, the dynamics of the full problem, as it is the case for the average one.

4. Beyond the quadratic approximation: Birkhoff’s normal form and family of periodic orbits

Let us begin with the study of the dynamics in the neighborhood of L_4 (the discussion would be the same at L_5). We first start with the linearized system at this point, or equivalently, with the quadratic expansion of the average Hamiltonian in the vicinity of L_4 . Using the notations (17) and (34), this expansion takes the form

$$\eta_1\left(\theta - \frac{\pi}{3}\right)^2 + \eta_2 u^2 + H_2^{(h)}, \tag{50}$$

the coefficients η_1 and η_2 being deduced from (18). A symplectic diagonalization of the associated Hamiltonian system allows one to define a new canonical coordinate system $(z_0, \tilde{z}_0, z_1, \tilde{z}_1, z_2, \tilde{z}_2)$ that reduces the previous quadratic form to

$$K_2 = \sum_{q=0}^2 \gamma_q z_q \tilde{z}_q. \quad (51)$$

As for the variables x_j and \tilde{x}_j , the coordinates z_j and \tilde{z}_j are linked with the relation $\tilde{z}_j = -iz_j$. L_4 being an elliptic equilibrium point, the coefficients γ_j are purely imaginary. More precisely, we have $\gamma_0 = i\nu$, $\gamma_1 = ig_1$ and $\gamma_2 = ig_2 = 0$. Consequently, if $0 \leq j, k, l \leq 2$ are three distinct integers, the set defined by the equation $z_j = z_k = 0$ is a one-parameter family of periodic orbits of the linearized system parametrized by the complex number z_l . The frequency, which is given by $|\gamma_l|$, is the same for every orbit of the family. Let us denote \mathcal{F}_0 the family parametrized by z_0 that corresponds to the quasi-circular motions ($e_1 = e_2 = 0$). The one parametrized by z_1 corresponding to the linear approximation of the Anti-Lagrange orbits will be denoted \mathcal{F}_1^l . And the last one, governed by z_2 , which contains the Lagrangian elliptic configurations, will be symbolized by \mathcal{F}_2 .

Let us now consider the term of degree greater than two in the expansion of the average Hamiltonian in the neighborhood of L_4 , and let us write this expansion as

$$K = K_2 + \sum_{p \geq 3} K_p \text{ with } K_p = \sum_{\mathbf{q} \in \mathcal{D}_{6,p}} \gamma_{\mathbf{q}} z_0^{q_0} \tilde{z}_0^{\tilde{q}_0} z_1^{q_1} \tilde{z}_1^{\tilde{q}_1} z_2^{q_2} \tilde{z}_2^{\tilde{q}_2}, \quad (52)$$

where

$$\mathcal{D}_{2n,p} = \{\mathbf{q} = (q_0, \tilde{q}_0, \dots, q_{n-1}, \tilde{q}_{n-1}) \in \mathbb{N}^{2n} / |\mathbf{q}| = \sum_{j=0}^{n-1} (|q_j| + |\tilde{q}_j|) = p\}. \quad (53)$$

All the coefficients \mathbf{q} are not allowed in the summations (52): as $|x_1|^2 + |x_2|^2 = |z_1|^2 + |z_2|^2$ the D'Alembert rule is still valid in coordinates z_j , and the non-zero coefficients $\gamma_{\mathbf{q}}$ verify the relation $q_1 + q_2 = \tilde{q}_1 + \tilde{q}_2$. This last relation imposes that the total degree of the monomials $z_1^{q_1} \tilde{z}_1^{\tilde{q}_1} z_2^{q_2} \tilde{z}_2^{\tilde{q}_2}$ is even, thus, the manifold given by the equation $z_1 = z_2 = 0$ is still invariant by the flow of the Hamiltonian K defined in (52). It turns out that the family \mathcal{F}_0 is not only an invariant set of the linear problem (51) but also of the full average Hamiltonian (52). This statement also holds for the family \mathcal{F}_2 including Lagrange's configurations. Indeed, as we know that these configurations exist as fixed points of the average problem and that we always have $\theta = \pi/3$ and $a_1 = a_2$ (or $u = 0$), $z_0 = 0$ along the family \mathcal{F}_2 . In addition, the relations $\Delta\varpi = \pi/3$ and $e_1 = e_2 = \text{constant}$ impose that $z_1 = 0$, according to Section 3.1.1. This implies additional constraints on the coefficients of the Hamiltonian K . Indeed, as every element of this family is an equilibrium point, the Hamiltonian K fulfills the conditions $\frac{\partial K}{\partial z_j} = \frac{\partial K}{\partial \tilde{z}_j} = 0$ when $|z_0| = |z_1| = 0$. This is equivalent to the cancellation of the coefficients of the terms

$$(z_2 \tilde{z}_2)^{q_2}, z_0 (z_2 \tilde{z}_2)^{q_2}, \tilde{z}_0 (z_2 \tilde{z}_2)^{q_2}, z_1 \tilde{z}_2 (z_2 \tilde{z}_2)^{q_2}, \tilde{z}_1 z_2 (z_2 \tilde{z}_2)^{q_2}. \quad (54)$$

As regards the Anti-Lagrange family, the relations $|z_0| = |z_2| = 0$, which characterizes its infinitesimal approximation \mathcal{F}_1^l does not hold. Indeed, if these previous relations are preserved by the linear flow of the system associated to K_2 , it is no more the case by the flow of K . If the Lyapunov center theorem (see Meyer and Hall (1992)) could be applied to K , it would show the existence of a one parameter family of periodic orbits originating at L_4 and tangent to \mathcal{F}_1^l , whose periods would be close to $2\pi/|\gamma_1|$ in the neighborhood of L_4 . Unfortunately, the coefficient γ_2 being equal to zero, the hypothesis of the latter are not fulfilled. To overcome this difficulty, we use a more elaborated method, based on the construction of a Birkhoff normal form.

As mentioned above, the use of the coordinates (z_j, \tilde{z}_j) , provides an elementary parametrization of the families \mathcal{F}_0 and \mathcal{F}_2 . It is possible to build a coordinate system $(\zeta_j, \tilde{\zeta}_j)$ for which the Anti-Lagrange family possesses the same kind of parametrization than the two other families, that is $|\zeta_0| = |\zeta_2| = 0$ and ζ_1 depending on the element of the family. This coordinate system can be chosen among one of those that reduce the Hamiltonian K to its Birkhoff's normal form. In this context, the Birkhoff transformation consists in the construction of canonical transformations that act on homogeneous polynomials of given degrees in order to eliminate non-resonant monomials. These are the monomials which are not of the form

$$z_0^{q_0} \tilde{z}_0^{q_0} z_1^{q_1} \tilde{z}_1^{q_1} z_2^{q_2} \tilde{z}_2^{q_2}. \quad (55)$$

More precisely, this transformation is performed iteratively, each step being dedicated to the normalization of a given degree. An elementary transformation is defined by the time-one map of the flow of an auxiliary Hamiltonian w_n defined as a solution of the equation

$$\gamma_0 \left(\tilde{\zeta}_0 \frac{\partial w_n}{\partial \tilde{\zeta}_0} - \zeta_0 \frac{\partial w_n}{\partial \zeta_0} \right) + \gamma_1 \left(\tilde{\zeta}_1 \frac{\partial w_n}{\partial \tilde{\zeta}_1} - \zeta_1 \frac{\partial w_n}{\partial \zeta_1} \right) = \Psi_n, \quad (56)$$

where Ψ_n contains non resonant monomials of degree n (see Morbidelli (2002)). This equation being linear, it can be solved monomial by monomial. The resolution of the equation (56) for $\Psi_n = z_0^{q_0} \tilde{z}_0^{q_0} z_1^{q_1} \tilde{z}_1^{q_1} z_2^{q_2} \tilde{z}_2^{q_2}$ introduces the divisor $\gamma_0(\tilde{q}_0 - q_0) + \gamma_1(\tilde{q}_1 - q_1)$. If we assume that γ_0 and γ_1 are rationally independent, which is generically the case³, the denominator cancels only if $q_0 = \tilde{q}_0$ and $q_1 = \tilde{q}_1$ independently of q_2 and \tilde{q}_2 . Using the D'Alembert rule, the only monomials involving divisors equal to zero are $z_0^{q_0} \tilde{z}_0^{q_0} z_1^{q_1} \tilde{z}_1^{q_1} z_2^{q_2} \tilde{z}_2^{q_2}$ which are not eliminated from the Hamiltonian. Consequently, the Birkhoff normal form can be computed at any degree. Let us denote by $(\zeta_j, \tilde{\zeta}_j)$ the normalizing coordinates. By construction, the coordinates (z_j, \tilde{z}_j) and $(\zeta_j, \tilde{\zeta}_j)$ are related by expressions of the form: $z_j = \zeta_j + \mathcal{O}_2(\zeta_j, \tilde{\zeta}_j)$ with $\tilde{\zeta}_j = -i\bar{\zeta}_j$. Then the Hamiltonian reduced to a Birkhoff normal form reads

$$N(\zeta_j, \tilde{\zeta}_j) = \sum_{q=0}^2 \gamma_q \zeta_p \tilde{\zeta}_p + \sum_{q_0+q_1+q_2 \geq 2} \gamma'_q (\zeta_0 \tilde{\zeta}_0)^{q_0} (\zeta_1 \tilde{\zeta}_1)^{q_1} (\zeta_2 \tilde{\zeta}_2)^{q_2}, \quad (57)$$

where the γ'_q are complex numbers such that the coefficients of the monomials $(\zeta_2 \tilde{\zeta}_2)^{q_2}$ vanish. As an example, the Birkhoff normal form corresponding to $m_1 = m_J$ and $m_2 = m_S$ computed up to the fourth degree in $\zeta_j, \tilde{\zeta}_j$ reads

$$\begin{aligned} & -0.093622 i \zeta_0 \tilde{\zeta}_0 - 0.00439 i \zeta_1 \tilde{\zeta}_1 - 2450.55 \zeta_0^2 \tilde{\zeta}_0^2 + 472.218 \zeta_0 \tilde{\zeta}_0 \zeta_1 \tilde{\zeta}_1 \\ & + 253.10 \zeta_0 \tilde{\zeta}_0 \zeta_2 \tilde{\zeta}_2 - 38.0734 \zeta_1^2 \tilde{\zeta}_1^2 - 1.17035 \zeta_1 \tilde{\zeta}_1 \zeta_2 \tilde{\zeta}_2, \end{aligned} \quad (58)$$

where only a few digits of the coefficients are given here. Remark that the “linear” fundamental frequencies, namely the coefficients of the monomials $i \zeta_0 \tilde{\zeta}_0$ and $i \zeta_1 \tilde{\zeta}_1$, are negative real numbers. As it is more convenient to deal with positive quantities, we have decided to change the sign of these frequencies in the previous sections. In the coordinates $(\zeta_j, \tilde{\zeta}_j)$, the Hamiltonian system associated to N is trivially integrable. In particular, its phase space is foliated in 3-dimensional invariant tori carrying linear flows. In other words, using the angle-action variables (φ_j, I_j) defined by the relations $\zeta_j = \sqrt{I_j} e^{i\varphi_j}$, one can verify that the actions I_j are integrals of the motion, and that every solution is quasi-periodic with fundamental frequencies equal

³As $\gamma_1/\gamma_0 \sim \sqrt{27(m_1 + m_2)/m_0}/4$, only high order resonances can occur. This allows one to build the normal form up to a high degree, typically of order $1/\sqrt{\varepsilon}$. In our numerical application, the first potential small denominator involves terms of degree 48.

to $\omega_j = \frac{\partial N}{\partial I_j}$. Among these solutions, we focus now on those that are members of the families \mathcal{F}_j , that is the solutions satisfying the relations $I_k = I_l = 0$ (j, k, l pairwise distinct), or equivalently $\zeta_k = \zeta_l = 0$. Using the transformation that reduces the Hamiltonian K to its normal form up to a given degree, say $2n$, and taking into account the symmetries of the transformation⁴, one can show that the families are parametrized as follows. The family \mathcal{F}_0 containing the quasi-circular periodic orbits is given by

$$z_0 = \zeta_0 + f(\zeta_0, \tilde{\zeta}_0), z_1 = z_2 = 0, \tilde{\zeta}_0 = -i\bar{\zeta}_0 \in \mathbb{C}, \quad (59)$$

$f(\zeta_0, \tilde{\zeta}_0)$ being a polynomial of degree $2n$ in $(\zeta_0, \tilde{\zeta}_0)$ whose lower order terms are quadratic. The family \mathcal{F}_1 associated to the Anti-Lagrange orbits reads

$$z_0 = P(\zeta_1 \tilde{\zeta}_1), z_1 = \zeta_1 + \zeta_1 Q(\zeta_1 \tilde{\zeta}_1), z_2 = \zeta_1 R(\zeta_1 \tilde{\zeta}_1), \quad (60)$$

where P, Q and R are polynomials of a single complex variable of degree n whose lower order term is of degree one. Of course, we still have $\tilde{\zeta}_1 = -i\bar{\zeta}_1 \in \mathbb{C}$. As mentioned above, the elliptic equilateral configurations \mathcal{F}_2 are still given by:

$$z_0 = z_1 = 0, z_2 = \zeta_2, \zeta_2 = -i\bar{\zeta}_2 \in \mathbb{C}. \quad (61)$$

\mathcal{F}_1 is the most interesting of these three families. Indeed, the quasi-circular family \mathcal{F}_0 is well known and its orbits are already represented in the figures 1 and 2. The elliptic equilateral configurations \mathcal{F}_2 has also been extensively studied since their discovery by Lagrange. In addition, its expression in terms of elliptic elements is well known since it corresponds to $a_1 = a_2$, $e_1 = e_2$ and $\theta = \Delta\varpi = \pi/3$ (or $-\pi/3$ for the family starting from L_5). On the contrary, the family \mathcal{F}_1 has been only partially studied by Giuppone et al. (2010) and Hadjidemetriou and Voyatzis (2011).

The use of a Birkhoff normal form allows one to get any desired information concerning this family, providing that the orbits of the family are contained inside the domain of validity of the normal form. Practically, this is not the case for the whole family, at least some portion of \mathcal{F}_1 including L_4 is contained in such a domain. In order to estimate this region, we have computed the relative difference between K and N along \mathcal{F}_1 using the expression

$$\rho(\zeta_1) = \frac{|K(z_0, z_1, z_2, \tilde{z}_0, \tilde{z}_1, \tilde{z}_2) - N(0, \zeta_1, 0, 0, \tilde{\zeta}_1, 0)|}{|N(0, \zeta_1, 0, 0, \tilde{\zeta}_1, 0)|}, \quad (62)$$

where the values of z_j are deduced from ζ_1 by the relations (60). As $\rho(0) = 0$, and in order to be consistent with the approximations done during the computation of the average Hamiltonian, we consider that the normal form is relevant while $\rho(\zeta_1) < \varepsilon^2$. We have estimated that the thirtieth degree was a good compromise between the precision of the normal form and its number of terms. Once defined this domain in which the normal form is relevant, a linear transformation allows one to express the z_j (deduced from ζ_j) in terms of θ, u, x_1, x_2 and to deduce the expression of \mathcal{F}_1 with the help of the elliptic elements. This is shown on the left panel of the figure 4 in the particular cases $m_1 = m_J, m_2 = m_S$. Fig. 4.a displays the evolution of the eccentricity e_1 versus e_2 along the family \mathcal{F}_1 (red curve). The maximal value of e_2 for which the condition $\rho(\zeta_1) < \varepsilon^2$ (here $\rho(\zeta_1) < 10^{-6}$) is fulfilled is $e_2 = 0.23$, which corresponds to $e_1 \approx 0.066$. Let us note that, we have $\rho(\zeta_1) < 3 \times 10^{-16}$ as long as $e_2 < 0.12$ and that the precision obtained using the Birkhoff normal form is comparable to the machine epsilon. In this domain, e_1 seems to depend linearly on e_2 , the slope of the (red) line being equal to m_2/m_1 . The difference between the green curve, which shows the variation

⁴It is not necessary to detail this transformation, but the key point lies on the fact that it takes the form $\zeta_j = z_j + f_j(z_1, z_2, z_3, \tilde{z}_1, \tilde{z}_2, \tilde{z}_3)$ where the polynomial f_j possesses the same symmetries as $\frac{\partial K}{\partial \tilde{z}_j}$.

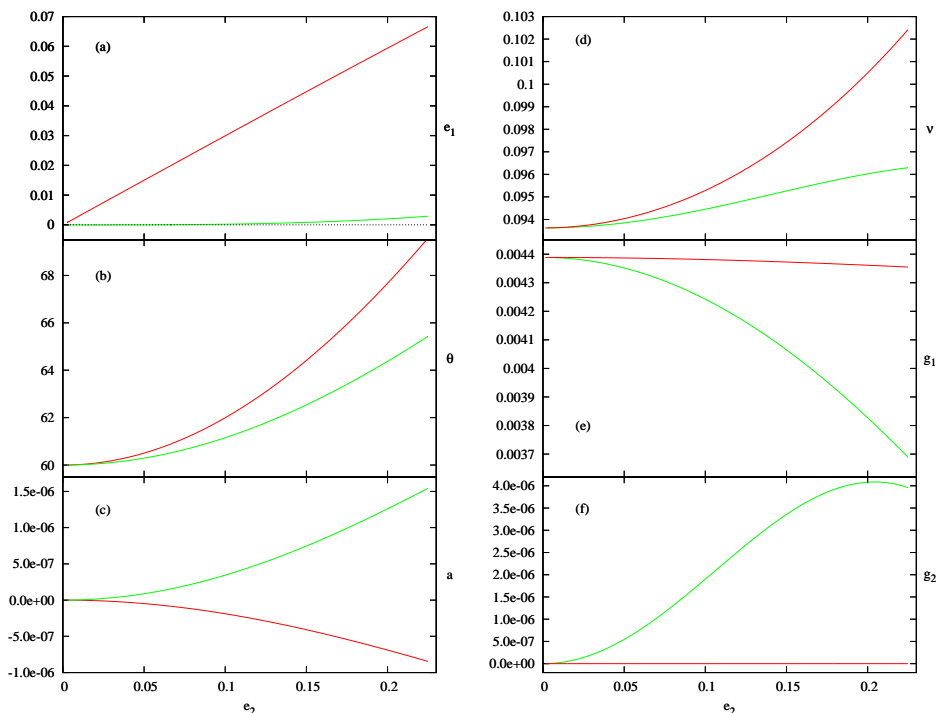


Fig. 4.— Evolution of the elliptic elements and of the fundamental frequencies in function of e_2 , along the families \mathcal{F}_1 and \mathcal{F}_2 . Left panel: elliptic elements. e_1 red curve, panel (a). θ in red and $\Delta\varpi$ (green) in panel (b). Panel (c): $a_1 - 1$ (red), $a_2 - 1$ (green). Right panel: the fundamental frequencies ν , g_1 and g_2 are represented in (d), (e) and (f). The green curves correspond to frequencies computed along \mathcal{F}_1 , \mathcal{F}_2 in red.

of $m_1 e_1 - m_2 e_2$ versus e_2 , and the dashed black line ($e_1 = 0$), indicates that the relation $m_1 e_1 = m_2 e_2$ is fulfilled only at the origin of the family \mathcal{F}_1 . Hadjidemetriou and Voyatzis (2011) suggest that along this family, e_1 and e_2 tend simultaneously to one regardless of the planetary masses. Fig. 4.b shows how the angles θ in red and $\Delta\varpi - 180^\circ$ in green move away from their value at the origin when e_2 increases. Basing on numerical simulations, Hadjidemetriou and Voyatzis (2011) suggest that the angles θ and $\Delta\varpi$ tend to 180° , when the eccentricities tend to one, which would correspond to a triple collision. The last figure of the left panel, Fig. 4.c, shows the slight deviation of the semi-major axes from the equality $a_1 = a_2 = 1$. Practically, $a_1 - 1$ is plotted in red, while the green curve corresponds to $a_2 - 1$. This figure shows that, at least for $e_2 < 0.23$, the variations of the semi-major axes are very small (of order ε^2) compared to the other elliptic elements. The situation may be different for large values of the eccentricities, but this is not mentioned in the literature.

Remark that, with the help of the analytical expression of \mathcal{F}_1 , we analyze a relatively small portion of the family \mathcal{F}_1 compared to the region studied numerically in Giuppone et al. (2010) and Hadjidemetriou and Voyatzis (2011) where the eccentricities reach 0.8. In contrast, our analytical study allows us to access to more information. First, it provides a complete understanding of the dynamics of all quasi-periodic trajectories lying in the validity domain of the Birkhoff normal form. Second, using an analytical expansion

of the eigenvectors of the differential system (38), we can establish rigorously that, at the beginning of the family \mathcal{F}_1 , the orbits satisfy the relation $m_1 e_1 = m_2 e_2$, which has been empirically deduced from numerical simulations in Giuppone et al. (2010). Third, it allows us to compute straightforwardly the fundamental frequencies associated to each trajectory belonging to a given family. Indeed, for \mathcal{F}_l , the derivative of the normal form N with respect to I_l is the frequency of the corresponding periodic orbit of the family (this frequency is zero in the particular case of \mathcal{F}_2). The normal frequencies are obtained by derivation with respect to the two other action variables. These three frequencies are plotted in Fig.4.d-f for the families \mathcal{F}_1 and \mathcal{F}_2 . The fundamental frequencies associated to the family \mathcal{F}_0 are not represented here for the simple reason that the normal form furnishes the same values as in figure 3, at least in a neighborhood of the circular equilateral configuration L_4 . The frequency ν (resp. g_1, g_2) is plotted in Fig. 4-d (reps. 4-e, 4-f). The red curves correspond the equilateral family \mathcal{F}_2 while the green curves are associated to \mathcal{F}_1 .

Although these frequencies and their derivatives are equal at the origin of the families, their behaviors along \mathcal{F}_1 and \mathcal{F}_2 are very different. As shown Fig. 4-f, the frequency g_2 is obviously equal to zero all along the Lagrange family since these trajectories are fixed points of the average problem. On the contrary, computed on the family \mathcal{F}_1 this frequency increases to a (local) maximum although it remains small in the considered interval. According Fig. 4-e, g_1 changes only very slightly for the equilateral family, but very much for \mathcal{F}_1 . Remark that the quantity $2\pi/g_1$, which seems to increase with the distance to L_4 , is the period of the orbits belonging to \mathcal{F}_1 . Regarding ν (Fig. 4-d), the frequency associated to \mathcal{F}_1 seems to reach a local maximum, while the one corresponding to \mathcal{F}_2 increases.

What can be said concerning the behavior of the fundamental frequencies outside of the validity domain of the normal form? One thing is clear about the equilateral configurations: when their eccentricity increases, a critical value depending on the mass ratio $(m_0 m_1 + m_0 m_2 + m_1 m_2)/(m_0 + m_1 + m_2)^2$ is reached, leading to a period-doubling bifurcation where the family loses its stability (Roberts 2002; Nauenberg 2002). Consequently, for $e_2 > 0.23$, the frequency ν is supposed to keep increasing, until it reaches the resonance $2\nu = n$, where n is the planetary mean motion (close to one if $\bar{a} = \mathcal{G} = m_0 = 1$). This is certainly the mechanism that was acting when Giuppone et al. (2010) observed the shrinking of the stable region surrounding the equilateral equilibrium, and finally its fading when the eccentricity grows. The way that the family \mathcal{F}_1 ends is less clear. In fact, at high eccentricities, only numerical simulations of these orbits have been performed (Giuppone et al. 2010; Hadjidemetriou and Voyatzis 2011), and when e does not exceed 0.8. Hadjidemetriou and Voyatzis (2011) suggest that for high eccentric orbits, the two eccentricities coincide, and that θ and $\Delta\varpi$ tend to π . This would imply that the Anti-Lagrange family \mathcal{F}_1 , and the Euler family originating at L_3 intersect, or end at a triple collision. This conjecture has to be checked.

5. Concluding remarks

In this paper, we developed a Hamiltonian formalism adapted to study the motion of two planets in co-orbital resonance. This analytical formalism intends to unify several works dedicated to the 1:1 mean-motion resonances like the formulations developed by Érdi (1977) or Morais (1999, 2001) in the case of the RTBP, but also models obtained by Dermott and Murray (1981a) and Yoder et al. (1983) aiming to understand the dynamics of the two Saturn’s satellites Janus and Epimetheus.

Our approach consists on an expansion of the average Hamiltonian in power series of both planetary eccentricities and inclinations. To make the study of the tadpole orbits as well as the horseshoe orbits possible, an expression of the mutual distance valid for all values of $\theta = \lambda_1 - \lambda_2$ has been introduced in

the Hamiltonian. Contrary to the other authors who modeled the distance between the two planets by the term $\sqrt{2 - 2 \cos \theta}$, we have chosen to introduce the divisor $\sqrt{a_1^2 + a_2^2 - 2a_1a_2 \cos \theta}$. This changes drastically the topology of the integrable problem associated to $e_1 = e_2 = I_1 = I_2 = 0$. Indeed, the usual model, which possesses three fixed points corresponding to L_3 , L_4 and L_5 , is singular when $\theta = 0$, regardless of the planetary semi-major axes values. Our approximation gives rise to two additional fixed points corresponding to the Euler points L_1 and L_2 . The singularity, that is usually identified to a line in the usual model, is here reduced to a single point that corresponds to the collision of the two planets in the same circular orbit, that is $a_1 = a_2, \theta = 0$. Thus, the topology of the two problems is very different. Indeed, with the first approximation, the phase space is divided in three distinct regions: two symmetrical libration regions around L_4 and L_5 respectively, and a third one, populated with horseshoe orbits that encompass the three equilibrium. Inside this last region, the semi-major axes tend to infinity when the angle θ approaches zero, which is obviously not very realistic. With the average model presented in this paper, the two regions surrounding L_4 and L_5 are practically the same as in the usual model, while the horseshoe region bounded in a domain lying between the separatrix emanating from L_3 and the one originated from L_2 . This model can be useful to simulate captures or transitions between different kinds of trajectories under the influence of weak dissipations, or slow migrations. Indeed, contrary to the usual model, the non-resonant region is better separated than the resonant horseshoe region.

For small eccentricities, the global topology of the problem is similar to the one described in Nesvorný et al. (2002) in the RTBP framework, using numerical averaging methods which are not limited to moderate eccentricities and inclinations. Although we are constrained by the size of eccentricities and inclinations, our model possesses at least two advantages. On the one hand, this average problem, as long as the number of terms of its Hamiltonian is not too large, allows fast numerical simulations using large time-steps. On the other hand, the present analytical formulation of the problem can help to obtain theoretical results concerning the stability inside the co-orbital resonance. If much has been done in the vicinity of the equilateral equilibrium points, especially in the RTBP (see Gabern et al. (2005) and references therein), the theoretical stability of horseshoe orbits remains an open problem.

With the help of a Birkhoff normal form, we have shown how the equilateral family \mathcal{F}_2 and the Anti-Lagrange family \mathcal{F}_1 bifurcate from the circular equilateral configuration L_4 . If the behavior of the family \mathcal{F}_2 is well known from its beginning at L_4 to its termination by a period-doubling bifurcation (Roberts 2002), the same cannot be said for the family \mathcal{F}_1 . At this point, we only have conjectures concerning the termination of this family. This might be a triple collision, and could be related to the end of the Euler aligned configurations originated at L_3 . A similar question, which is not discussed in the present paper, concerns the so-called quasi-satellites family (see Hadjidemetriou et al. (2009); Giuppone et al. (2010)) which could also end by collisions when the eccentricities tend to one (an alternation of two kinds of double collisions involving on the one hand, Sun and a first planet, and on the other hand, the second planet and the Sun).

A last point should be mentioned. In Section 3.1, the vertical variational equation has been set aside because the quadratic part of Hamiltonian in inclination was equal to zero. A careful study of this situation would reveal interesting bifurcation phenomena giving rise to families of remarkable orbits, as in the case of the RTBP (Perdios and Zagouras 1991; Marchal 2009) or in the general three-body problem with equal masses (Chenciner and Féjóz 2008). Finally, a lot remains to be done in that field.

6. Appendix: L_4 in heliocentric canonical elliptic elements

Let us assume that the three bodies describe a circular Lagrangian equilateral configuration where ρ is the length of the triangle sides. The heliocentric coordinate system can be chosen such as $\mathbf{r}_j = \rho \mathbf{u}_j$ where

$$\mathbf{u}_j = \begin{pmatrix} \cos \varphi_j \\ \sin \varphi_j \\ 0 \end{pmatrix}, \quad \text{with } \varphi_1 = \omega t \text{ and } \varphi_2 = \omega t + \frac{\pi}{3}, \quad (63)$$

the angular velocity ω of the relative equilibrium satisfying the third Kepler law $\omega^2 \rho^3 = \mu = \mathcal{G}(m_0 + m_1 + m_2)$. The elliptic elements $(a_j, e_j, v_j, \varpi_j)$ can be derived from the canonical heliocentric coordinates $(\tilde{\mathbf{r}}_j, \dot{\mathbf{r}}_j)$ using the relations

$$K_j = \frac{\tilde{\mathbf{r}}_j^2}{2\beta_j} - \frac{\mu_j \beta_j}{\|\mathbf{r}_j\|} = -\frac{\beta_j \mu_j}{2a_j}, \quad (64)$$

$$\mathbf{E}_j = \mu_j^{-1} \frac{\tilde{\mathbf{r}}_j}{\beta_j} \times \left(\mathbf{r}_j \times \frac{\dot{\mathbf{r}}_j}{\beta_j} \right) - \mathbf{u}_j = e_j \begin{pmatrix} \cos \varpi_j \\ \sin \varpi_j \\ 0 \end{pmatrix} \quad (65)$$

and

$$\cos v_j = e_j^{-1} \mathbf{E}_j \cdot \mathbf{u}_j. \quad (66)$$

$$\frac{\tilde{\mathbf{r}}_j}{\beta_j} = \gamma^{-1} \left(\dot{\mathbf{r}}_j - \frac{\beta_k}{m_0} \dot{\mathbf{r}}_k \right), \quad \text{with } \gamma = 1 - \frac{\beta_1 \beta_2}{m_0^2}, \quad (j, k) \in \{1, 2\} \quad \text{and} \quad j \neq k, \quad (67)$$

a straightforward computation leads to the expressions

$$K_j = -\frac{\beta_j \mu_j}{2\rho} \left(2 - \frac{\mu}{\mu_j} \left(1 - \frac{\beta_k}{m_0} + \frac{\beta_k^2}{m_0^2} \right) \gamma^{-2} \right) \quad (68)$$

and

$$\gamma^2 \mathbf{E}_j = \left(\frac{m_k}{m_0 + m_j} - \frac{1}{2} \frac{\mu}{\mu_j} \frac{\beta_k}{m_0} \right) \mathbf{u}_j + \frac{\mu}{\mu_j} \frac{\beta_k}{m_0} \left(\frac{1}{2} \frac{\beta_k}{m_0} - 1 \right) \mathbf{u}_k. \quad (69)$$

According to (68), the semi-major axis of the planet j is a time-independent quantity approximated by the expression

$$a_j = \rho \left(1 + \frac{m_k}{m_0} \frac{m_1 + m_2}{m_0} + \mathcal{O}(\varepsilon^3) \right) \quad (70)$$

which is slightly larger than the radius ρ of the configuration. As $\mathbf{u}_1 \cdot \mathbf{u}_2 = 1/2$, the expression (69) shows that the eccentricity (modulus of \mathbf{E}_j) is constant, and that the ellipse rotates with an angular velocity equal to ω . A first order expansion of (69) gives

$$\mathbf{E}_j = \frac{m_k}{m_0} \left(\frac{\mathbf{u}_j}{2} - \mathbf{u}_k \right) + \mathcal{O}(\varepsilon^2) \quad (71)$$

and

$$e_j = \frac{\sqrt{3}}{2} \frac{m_k}{m_0} + \mathcal{O}(\varepsilon^2). \quad (72)$$

We deduced from (66) that the true anomalies v_j of the planets satisfy

$$\cos v_j = \frac{4m_j + m_k}{2\sqrt{3}m_0} + \mathcal{O}(\varepsilon^2). \quad (73)$$

REFERENCES

- Barrarés, E., Ollé, M.: Invariant manifolds of L_3 and horseshoe motion in the restricted three-body problem. *Nonlinearity* **19**, 2065–2089 (2006)
- Chenciner, A.: Poincaré and the three-body problem. In *Séminaire Poincaré (Bourbaphy) XVI : Poincaré, 1912-2012*, pp 45–133 (2012)
- Chenciner, A., Féjoz, J.: The flow of the equal-mass spatial 3-body problem in the neighborhood of the equilateral relative equilibrium. *Discrete and Continuous Dynamical Systems, Series B* **10**, 421–438 (2008)
- Chenciner, A., Féjoz, J.: Unchained polygons and the n-body problem. *Regular and Chaotic Dynamics* **14**, 64–115 (2009)
- Christou, A. A.: A Numerical Survey of Transient Co-orbitals of the Terrestrial Planets. *Icarus* **144**, 1–20 (2000)
- Dermott, S. F., Murray, C. D.: The dynamics of tadpole and horseshoe orbits. I - Theory. II - The coorbital satellites of Saturn. *Icarus* **48**, 1–11 (1981a)
- Dermott, S. F., Murray, C. D.: The dynamics of tadpole and horseshoe orbits II. The coorbital satellites of saturn. *Icarus* **48**, 12–22 (1981b)
- Dvorak, R.: Exchange orbits in planetary systems. In Suli A., Freistetter F., Pal A., editor, *Proc. Fourth Austrian Hungarian Workshop on Celestial Mechanics.*, pp 63–74 (2006)
- Érdi, B.: An asymptotic solution for the trojan case of the plane elliptic restricted problem of three bodies. *Celest. Mech. Dyn. Astron.* **15**, 367–383 (1977)
- Gabern, F., Jorba, A., Locatelli, U.: On the construction of the Kolmogorov normal form for the Trojan asteroids. *Nonlinearity* **18**, 1705–1734 (2005)
- Garfinkel, B.: A theory of libration. *Celestial Mechanics* **13**, 229–246 (1976)
- Garfinkel, B.: Theory of the Trojan asteroids. I. *Astron. J.* **82**, 368–379 (1977)
- Garfinkel, B.: Theory of the Trojan asteroids. II. *Celestial Mechanics* **18**, 259–275 (1978)
- Gascheau, G.: Examen d’une classe d’équations différentielles et application à un cas particulier du problème des trois corps. *Compt. Rend.* **16**(7), 393–394 (1843)
- Giuppone, C. A., Beaugé, C., Michtchenko, T. A., Ferraz-Mello, S.: Dynamics of two planets in co-orbital motion. *MNRAS* **407**, 390–398 (2010)
- Greenberg, R.: Apsidal precession of orbits about an oblate planet. *Astron. J.* **86**, 912–914 (1981)
- Hadjidemetriou, J. D., Psychoyos, D., Voyatzis, G.: The 1/1 resonance in extrasolar planetary systems. *Celest. Mech. Dyn. Astron.* **104**, 23–38 (2009)
- Hadjidemetriou, J. D., Voyatzis, G.: The 1/1 resonance in extrasolar systems. Migration from planetary to satellite orbits. *Celest. Mech. Dyn. Astron.* **111**, 179–199 (2011)

- Jorba, À.: A numerical study on the existence of stable motions near the triangular points of the real earth-moon system. *Astron. Astrophys.* **364**, 327–338 (2000)
- Laskar, J., Robutel, P.: Stability of the planetary three-body problem I: Expansion of the planetary hamiltonian. *Celest. Mech. Dyn. Astron.* **62**, 193–217 (1995)
- Laughlin, G., Chambers, J. E.: Extrasolar Trojans: The Viability and Detectability of Planets in the 1:1 Resonance. *Astron. J.* **124**, 592–600 (2002)
- Malige, F., Robutel, P., Laskar, J.: Partial reduction in the n-body planetary problem using the angular momentum integral. *Celest. Mech. Dyn. Astron.* **84**, 283–316 (2002)
- Marchal, C., Bozis, G.: Hill Stability and Distance Curves for the General Three-Body Problem. *Celestial Mechanics* **26**, 311–333 (1982)
- Marchal, C.: Long term evolution of quasi-circular Trojan orbits. *Celest. Mech. Dyn. Astron.* **104**, 53–67 (2009)
- Meyer, K. R. and Hall, G. R.: Introduction to Hamiltonian dynamical systems and the n-body problem. Springer-Verlag. (1992)
- Morais, M. H. M.: A secular theory for Trojan-type motion. *Astron. Astrophys.* **350**, 318–326 (1999)
- Morais, M. H. M.: Hamiltonian formulation of the secular theory for Trojan-type motion. *Astron. Astrophys.* **369**, 677–689 (2001)
- Morbidelli, A.: Modern celestial mechanics : aspects of solar system dynamics. Taylor & Francis, London, 2002, ISBN 0415279399 (2002)
- Nauenberg, M.: Stability and Eccentricity for Two Planets in a 1:1 Resonance, and Their Possible Occurrence in Extrasolar Planetary Systems. *Astron. J.* **124**, 2332–2338 (2002)
- Nesvorný, D., Thomas, F., Ferraz-Mello, S., Morbidelli, A.: A perturbative treatment of the co-orbital motion. *Celest. Mech. Dyn. Astron.* **82**, 323–361 (2002)
- Perdios, E. and Zagouras, C. G.: Vertical stability of periodic solutions around the triangular equilibrium points. *Celest. Mech. Dyn. Astron.* **51**, 75–81 (1991)
- Poincaré, H.: *Méthodes nouvelles de la Mécanique Céleste*, volume I. Gauthier Villars Paris, reprinted by Blanchard, 1987 (1892)
- Poincaré, H.: *Leçons de Mécanique Céleste*, tome I. Gauthier Villars Paris, (1905)
- Roberts, G.: Linear stability of the elliptic Lagrangian triangle solutions in the three-body problem. *J. Differential Equations* **182**, 191–218 (2002)
- Robutel, P.: Stability of the planetary three-body problem II: Kam theory and existence of quasiperiodic motions. *Celest. Mech. Dyn. Astron.* **62**, 219–261 (1995)
- Roy, A.: *Orbital motion*. Bristol : A. Higell. (1982)
- Sicardy, B. and Dubois, V.: Co-Orbital Motion with Slowly Varying Parameters. *Celest. Mech. Dyn. Astron.* **86**, 321–350 (2003)

- Smith, B. A., Reitsema, H. J., Fountain, J. W., Larson, S. M.: Saturn's Inner Co-Orbital Satellites. In Bulletin of the American Astronomical Society, volume 12 of BAAS, pp 727 (1980)
- Synnott, S. P., Peters, C. F., Smith, B. A., Morabito, L. A.: Orbits of the small satellites of Saturn. Science **212**, 191 (1981)
- Szebehely, V.: Theory of orbits: the restricted problem of three bodies. Academic Press, New-York, (1967)
- Yoder, C. F., Colombo, G., Synnott, S. P., Yoder, K. A.: Theory of motion of Saturn's coorbiting satellites. Icarus **53**, 431–443 (1983)